Published in final edited form as:
Neuron. 2013 May 8; 78(3): 498–509. doi:10.1016/j.neuron.2013.02.036.

Autism-Associated Neuroligin-3 Mutations Commonly Disrupt Tonic Endocannabinoid Signaling

Csaba Földy[1,2], **Robert C. Malenka**[2,3], and **Thomas C. Südhof**[1,3,4]

[1]Department of Molecular and Cellular Physiology, Stanford University Medical School, Stanford, CA94305

[2]Nancy Pritzker Laboratory, Stanford University Medical School, Stanford, CA94305

[3]Department of Psychiatry, Stanford University Medical School, Stanford, CA94305

[4]Howard Hughes Medical Institute, Stanford University Medical School, Stanford, CA94305

Abstract

Neuroligins are postsynaptic cell-adhesion molecules that interact with presynaptic neurexins. Rare mutations in neuroligins and neurexins predispose to autism, including a neuroligin-3 amino-acid substitution (R451C) and a neuroligin-3 deletion. Previous analyses showed that neuroligin-3 R451C-knockin mice exhibit robust synaptic phenotypes, but failed to uncover major changes in neuroligin-3 knockout mice, questioning the notion that a common synaptic mechanism mediates autism pathogenesis in patients with these mutations. Here, we used paired recordings in mice carrying these mutations to measure synaptic transmission at GABAergic synapses formed by hippocampal parvalbumin- and cholecystokinin-expressing basket cells onto pyramidal neurons. We demonstrate that in addition to unique gain-of-function effects produced by the neuroligin-3 R451C-knockin but not the neuroligin-3 knockout mutation, both mutations dramatically impaired tonic but not phasic endocannabinoid signaling. Our data thus suggest that neuroligin-3 is specifically required for tonic endocannabinoid signaling, raising the possibility that alterations in endocannabinoid signaling may contribute to autism pathophysiology.

INTRODUCTION

Neuroligins are postsynaptic cell-adhesion molecules that are expressed in four principal isoforms (neuroligin-1 to -4, abbreviated as NL1 to NL4), and that act as ligands for presynaptic neurexins (Ichtchenko et al., 1995). NL1 is found in excitatory synapses (Song et al., 1999), NL2 in inhibitory synapses (Veroqueaux et al., 2004; Graf et al., 2004), NL3 in both (Budreck and Scheiffele, 2007), and NL4 in glycinergic synapses (Hoon et al., 2011). In humans, more than 30 neuroligin gene mutations have been associated with autism, including a NL3 point mutation (the R451C substitution; Jamain et al., 2003) and a NL3 deletion (Sanders et al., 2011).

Experiments with knockout (KO) mice revealed that neuroligins are essential for synaptic transmission, and suggest that neuroligins organize synapses and determine synapse

Address for correspondence: C.F. (foldy@stanford.edu) or T.C.S. (tcs1@stanford.edu).

properties (Varoqueaux et al., 2006). Specifically, triple KO mice lacking NL1, NL2, and NL3 die at birth because their synapses – although morphologically normal – exhibit severe impairments in synaptic transmission (Varoqueaux et al., 2006). Moreover, single KO mice lacking either NL1 or NL2 exhibit major deficits in excitatory or inhibitory synaptic transmission, respectively (Chubykin et al., 2007; Gibson et al., 2009; Poulopoulos et al., 2009). NL3 KO mice display changes in spontaneous `mini' synaptic events in the hippocampus (Tabuchi et al., 2007; Etherton et al., 2011a) and in mGluR5 signaling in the cerebellum (Baudouin et al., 2012). Together, these findings are consistent with the notion that neuroligins specify synaptic properties instead of functioning as general `glues' for synapses (Varoqueaux et al., 2006). These conclusions are additionally supported by characterization of another NL3 mutation, the R704C substitution (Etherton et al., 2011b). The R704C substitution corresponds to an autism-associated mutation in NL4 (Zhang et al., 2009) that, when introduced into NL3, selectively altered postsynaptic AMPA-type glutamate receptor levels, confirming that neuroligins contribute to shaping synapse properties.

In contrast to NL3 KO mice, NL3 knockin (KI) mice carrying the R451C substitution that mimics the human autism mutation displayed robust synaptic phenotypes that differed between the somatosensory cortex and hippocampus, and that were absent from NL3 KO mice (Tabuchi et al., 2007; Etherton et al., 2011a; see also Südhof, 2008). Thus, although the R451C substitution destabilizes NL3 (De Jaco et al., 2010) and caused a loss of more than 90% of NL3 protein (Tabuchi et al., 2007), it nevertheless produced a gain-of-function phenotype in at least some synapses. To date, no synaptic phenotype was detected that is shared by the two known autism-associated NL3 mutations, raising the question of how these mutations may actually induce autism.

To gain insight into how different NL3 mutations might contribute to autism pathogenesis, we here followed up on the observation that the NL3 KO increases inhibitory and decreases excitatory spontaneous mini events in the hippocampus (Etherton et al., 2011a). Since the NL3 KO did not alter excitatory synaptic strength in the hippocampus, we hypothesized that the NL3 KO may cause a specific change in a subset of inhibitory synapses. The hippocampus contains multiple at least 21 different types of inhibitory neurons that exhibit specific circuit properties (Klausberger and Somogyi, 2008). Thus, when examining inhibitory synaptic transmission, it is advantageous to investigate specific synapses formed by identified types of inhibitory neurons. To this end, we performed paired recordings that monitor synapses formed by two different defined types of inhibitory basket cells onto the soma and proximal dendrites of pyramidal neurons. One type of basket cell co-expresses presynaptic cannabinoid type-1 (CB1) receptors and the neuropeptide cholecystokinin (CCK; `CCK basket cells'), whereas the other type expresses parvalbumin (PV; `PV basket cells'; Freund, 2003; Freund et al., 2003; Bartos et al., 2007; Klausberger and Somogyi, 2008). The two types of basket cells participate in parallel inhibitory systems that play distinct but complementary roles in network oscillations (Bartos et a., 2007; Klausberger et al., 2005), and have been implicated in neurological and mood disorders (Freund and Katona, 2007; Lisman et al., 2008). In these paired recordings, we sought to identify specific loss-of-function effects that are shared by both the NL3 KO and the R451C KI mutation since both are associated with autism, prompting us to analyze both mutations in parallel.

Our data show that NL3 R451C KI and NL3 KO neurons exhibit distinct phenotypes at synapses formed by PV basket cells, similar to previous observations in other synapses (Tabuchi et al., 2007; Etherton et al., 2011a). Surprisingly, however, we find that at synapses formed by CCK basket cells, the two mutations produced the same phenotype that consisted of a loss of the tonic CB1 receptor-dependent suppression of GABA release that is observed at these synapses (Losonczy et al., 2004; Hentges et al., 2005; Neu et al., 2007; Ali and

Todorova, 2010; Kim and Alger, 2010). This observation identifies NL3 as the first molecule that is selectively essential for tonic endocannabinoid signaling, an enigmatic component of overall endocannabinoid signaling (Alger, 2012). Given the common genetic association of the R451C substitution and NL3 deletion with autism, our data thus suggest that disrupted endocannabinoid signaling may contribute to autism pathophysiology, a tantalizing idea given the great interest in developing therapeutic approaches that modify endocannabinoid signaling in the brain.

RESULTS

R451C KI impairs GABAergic synaptic transmission at PV basket cell synapses

We performed paired whole-cell recordings between presynaptic basket cells and postsynaptic CA1 pyramidal neurons in acute slices from littermate wild-type and R451C KI mice (Tabuchi et al., 2007). In these recordings, we determined the characteristics of synaptic transmission by measuring unitary inhibitory post-synaptic currents (IPSCs) evoked by basket cell action potentials (APs)(see Experimental Procedures for details).

We found that the R451C KI severely impaired synaptic transmission at synapses formed by PV basket cells onto pyramidal neurons (Figs. 1A and 1B). The amplitude of IPSCs was decreased ~70% (failures included), and the success rate with which an AP elicited an IPSC was lowered ~20%. This phenotype was observed independent of whether APs were induced at 1 Hz, 2 Hz, or 10 Hz. In addition, we observed a statistically insignificant decrease in IPSC half-widths (Fig. 1C, WT: 5 ± 0.3 ms, R451C: 4.3 ± 0.2 ms). The impairment of IPSCs in R451C KI neurons was independent of postsynaptic membrane potential (analyzed from −80 to +60 mV; Figs. 1E and S1), and the R451C KI did not affect the reversal potential of PV basket cell-evoked IPSCs (WT: −18.6 ± 1.9 mV, R451C: −19.4 ± 2.1 mV). Moreover, we observed no change in the amplitude of the minimal unitary IPSC that could be evoked by a presynaptic AP, suggesting that single synaptic events elicited similar postsynaptic responses (Fig. 1D; WT: 22.5 ± 3.5 pA, R451C: 16.4 ± 0.8 pA). We also found no change in the number of trials needed to identify synaptically connected pairs of PV basket cell/pyramidal neurons, indicating that the number of pyramidal neurons innervated by individual PV basket cells was not altered (Fig. 1F; WT: 1.8±0.3, R451C: 1.8±0.2 trials per presynaptic basket cell). Finally, we did not detect major morphological changes in the axonal or dendritic arbor of PV basket cells in R451C KI mice (Fig. 1G).

Together, these data show that the R451C KI produces a large impairment in synaptic transmission at synapses formed by PV basket cells onto pyramidal neurons. The lack of a change in the voltage-dependence of IPSCs, the reversal potential, and the minimal unitary IPSC size suggest that the R451C KI did not alter the number of postsynaptic GABA-receptors or disrupt postsynaptic chloride homeostasis, while the lack of change in the IPSC kinetics suggests that the subunit composition of GABA-receptors or the reuptake kinetics of released GABA were not altered significantly. The decrease in the success rate of eliciting an IPSC from PV basket cells suggests that the R451C KI impaired synaptic transmission by a presynaptic mechanism, despite the presumed postsynaptic localization of NL3. Notably, this is the first phenotype of the R451C mutation that entails a decrease in synaptic strength, not an increase as previously observed for global inhibitory synaptic transmission in the somatosensory cortex (Tabuchi et al., 2007) and for both AMPA- and NMDA-receptor mediated excitatory synaptic transmission in the hippocampus (Etherton et al., 2011a).

The R451C KI enhances GABAergic synaptic transmission at CCK basket cell synapses

We next analyzed the properties of transmission at pyramidal synapses formed by CCK basket cells. Surprisingly, here the R451C KI caused a ~100% increase in the IPSC amplitudes and a ~15% increase in the IPSC success rate during 1 Hz stimulation, and a slightly smaller change during 2 and 10 Hz stimulation (Figs. 2A and 2B). The increase in success rate suggests an increase in the presynaptic GABA release probability, which is also a plausible explanation for the increase in IPSC amplitudes. This hypothesis was further supported by the absence of detectable changes in the IPSC half-width, indicating that the GABA-receptor subunit composition or uptake mechanisms were unaltered (Fig. 2C; WT: 6.3±0.4 ms, R451C: 5.4±0.3 ms). Furthermore, the amplitude of minimal unitary IPSCs (Fig. 2D; WT: 23.4±4.3 pA, R451C: 29.6±4 pA) and the rate of finding connected pairs (Fig. 2E; WT: 2.6±0.7, R451C: 2.2±0.3) were similar in wild-type and R451C mutant slices, as was the morphology of their CCK basket cells (Fig. 2F). The phenotype of the R451C mutation in the CCK cell synapses again was more consistent with a presynaptic change (such as increased release probability) than a structural alteration (e.g. increase in synapse density) or postsynaptic effect. Thus, the R451C KI produces opposite changes at two different perisomatic inhibitory synapses, and in both cases the changes appear to involve an ultimately presynaptic mechanism, even though NL3 is a postsynaptic molecule.

A synaptic phenotype of NL3 KO mice

To test whether the R451C KI phenotypes represent gain- or loss-of-function effects, we next performed paired recordings in acute slices from NL3 KO mice, again using littermate wild-type mice as controls. When we analyzed the properties of transmission between PV basket cells and pyramidal neurons, we failed to detect a phenotype. Specifically, the amplitude and success rate of IPSCs were unchanged (Figs. 3A and 3B), as were the half-width of the IPSCs (Fig. 3C; WT: 4.7 ± 0.2 ms, NL3 KO: 5.5 ± 0.4 ms), the size of unitary minimal IPSCs (Fig. 3D; WT: 17.6±1.6 pA, NL3 KO: 16.5 ± 1.1 pA), and the rate of finding connected pairs (Fig. 3E; WT: 2.2 ± 0.3, NL3 KO: 2.5 ± 0.6). These results suggest that the loss of synaptic transmission at this synapse in R451C mutant mice represents an active suppression of synaptic transmission by a gain-of-function activity of R451C-mutant NL3.

We then examined the effect of the NL3 KO on synaptic transmission mediated by inhibitory synapses that were formed by CCK-containing terminals on pyramidal neurons (Fig. 4). Surprisingly, here the NL3 KO phenocopied the R451C KI. Specifically, the NL3 KO caused a significant increase in synaptic strength, as manifested by both an increase in IPSC amplitude and in success rate (Figs. 4A and 4B). In addition, we observed a small increase in IPSC half-width (Fig. 4C; WT: 4.9±0.1 ms, NL3 KO: 5.6±0.2), but no change in the size of unitary minimal IPSCs (Fig. 4D; WT: 25.3±1.7 pA, NL3 KO: 29±2.9 pA), or in the rate of finding synaptically connected pairs of neurons (Fig. 4E; WT: 2±0.2, NL3 KO: 1.8±0.2). The fact that increased synaptic transmission at CCK basket cell synapses is equally observed in NL3 KO and R451C KI neurons shows that it is caused by a loss-of-function mechanism.

NL3 R451C KI lowers the probability of GABA release at PV basket cell synapses

The change in success rates in our paired recordings of synapses with the NL3 R451C KI or the NL3 KO mutations suggests a presynaptic origin for the observed phenotypes, despite the postsynaptic localization of NL3 (Budreck and Scheiffele, 2007). To evaluate whether presynaptic changes alone (such as in the probability of release) could in principle account for the NL3 related phenotypes, we analyzed these phenotypes by modeling and computer simulations.

We first plotted bin-averaged PV basket cell IPSC amplitudes against their corresponding averaged success rates (Fig. 5A; inset shows distribution of individual pairs). We then fitted these data with an equation that relates IPSC amplitudes to the success rate of transmission ($\left[\mathrm{PSC}=\mathrm{Q}\cdot\mathrm{N}\cdot\left[1-\sqrt[N]{1-\mathrm{successes}}\right]\right.$ see Experimental Procedures and Figs. S2A–S2C) to estimate characteristic mean quantal size (Q) and number of release sites (N) for WT (n=25) and R451C KI (n=26) populations. The resulting estimates for Q were similar for both genotypes (mean and 95% confidence intervals: 21.9/12.5–31.3 pA and 17.5/16.4–18.6 pA for WT and R451C, respectively), as were the estimates for N (mean and 95% confidence intervals: 7.6/1.6–13.6 and 8.7/0–17.4 for WT and R451C synapses, respectively). These estimates support the notion that the synaptic phenotype in R451C-mutant PV basket cell synapses was not due to a decrease in quantal size (see Fig. 1D), and, limited by the wide confidence interval of estimates, also suggest that the R451C phenotype was not due to a decrease in the number of release sites.

To examine the remaining possibility, namely that a lower neurotransmitter release probability (P_R) underlies the R451C phenotype, we performed computer simulations in which we modeled IPSCs at different P_R values (Figs. 5B and S3). In this computational model, we incorporated a minimal set of synaptic parameters that allowed us to simulate the IPSC amplitudes and success rates, and to compare these parameters to the experimental data. The simulation parameters included, in addition to the number of release sites (N), the mean and the variance of the release probability (P_R and σ_{PR}) and the mean and the variance of the quantal amplitude (Q and σ_Q). For each simulated paired recording, the computationally determined IPSC (cIPSC) was derived as $cIPC=\sum_{i=1}^{N} p_i \cdot q_i$, and the computationally determined success rate (cSuccesses) was derived as $cSuccess=\left[1-\prod_{i=1}^{N}(1-p_i)\right]\cdot 100$, where p_i and q_i are the probability of release and the quantal amplitude in the *i*-th release site, respectively (see Experimental Procedures and Figs. S3A–3G).

We started the simulations by using Q and N values estimated from the population quantal analysis (Fig. 5A; see above) to derive values for P_R, σ_{PR}, and σ_Q that result in cIPSCs and cSuccesses which approximate the experimentally determined IPSCs and success rates. For PV basket cell IPSCs in WT neurons, we found that a P_R=0.23, together with a σ_{PR}=0.224 and a σ_Q=2.25 (Q=21 pA and N=7, per modeling), provided computationally determined cIPSCs and cSuccesses that did not significantly differ from the experimental data (mean difference ± SD for IPSCs: 0±6 pA; for success rates: 0±0.02; t-test, P>0.5 for both). For computer simulation of R451C synapses, we found that much lowered release probabilities, P_R=0.11, together with a σ_{PR}=0.09 and a σ_Q=1.65 (Q=17 pA and N=8, per modeling) were needed to replicate the experimental data (mean difference ± SD for IPSCs: 0±0.99 pA; for success rates: 0±0.01; t-test, P>0.5 for both). These simulations thus suggest that a ~2-fold decrease in the probability of GABA release could sufficiently explain the NL3 R451C KI phenotype in PV basket cell synapses. These conclusions were further supported by consequent analysis of biocytin-filled axons (Fig. 5C), which also did not indicate a difference in the number of synapses formed by individual PV basket cells (WT: 0.33±0.03 and R451C: 0.26±0.01, synapses per μm, Mann-Whitney RST, P=0.152).

Next, we sought to determine a cause for lower release rates in PV basket cell synapses in the R451C KI mice. We reasoned that such decreases in release rate could be caused by NL3 mutation-driven alterations of the presynaptic release machinery, or alternatively, by over-activation of a presynaptic receptor, such as a neuropeptide receptor, that physiologically suppresses GABA release from these synapses (Freund and Katona, 2007). We addressed

this latter possibility by application of pharmacological agents in paired recording experiments.

Activation of two presynaptic G-protein coupled receptors, namely μ-opioid and M2 muscarinic-receptors, is known to suppress GABA release at PV basket cell synapses (Glickfeld et al., 2008, Szabó et al., 2010). Thus, we tested the effect of the μ-opioid receptor antagonist CTAP (500 nM; Fig. 5D, n=4 pairs) and of the M2 muscarinic-receptor antagonist AF-DX (10 μM; Fig. 5E, n=4 pairs) in paired-recordings of PV basket cell to pyramidal neuron synapses in NL3 R451C KI mice. Neither antagonist increased IPSC amplitudes in paired recordings, indicating that tonic activation of these receptors does not account for the decreased transmission at PV basket cell synapses in R451C KI mice. In additional control experiments, both antagonists reliably reversed the effect of their corresponding agonists, DAMGO (1 μM) and carbachol (5 μM; not shown). Thus, the presence of NL3 the R451C mutation likely induces a functional change in the presynaptic release properties of PV basket cell synapses.

Neuroligin-3 is essential for tonic endocannabinoid signaling at CCK basket cell synapses

Our data suggest that a loss of NL3 function produces an increase in GABA release at synapses formed by CCK basket cells onto pyramidal neurons synapses. CCK basket cell synapses exhibit a distinct feature that offers an immediate hypothesis to account for the observed phenotype. This feature consists of the efficient suppression of GABA release from CCK basket cell terminals by the endocannabinoid-mediated activation of presynaptic CB1 receptors (reviewed in Alger, 2002; Piomelli, 2003; Freund and Katona, 2007).

Endocannabinoids are secreted from postsynaptic pyramidal neurons to activate presynaptic CB1 receptors in two principal modes. Phasic secretion of endocannabinoids is induced by postsynaptic depolarization and/or mGluR5 activation and mediates decreases in synaptic transmission during short- and long-term plasticity. Tonic secretion of endocannabinoids affects synaptic transmission over longer time periods (reviewed in Alger, 2012; Katona and Freund, 2012). A deficiency in tonic endocannabinoid signaling, with or without an effect on phasic endocannabinoid signaling, would be expected to enhance the probability of GABA release, and thus would increase IPSCs similar to what we observed in R451C KI and NL3 KO neurons. Thus, we tested the hypothesis that a loss-of-function of NL3 - either via the KO or via the R451C KI - impairs tonic endocannabinoid signaling.

In wild-type synapses, bath application of 10 μM AM251 (a CB1 receptor antagonist and inverse agonist) caused a ~100% increase in IPSC amplitudes and ~50% increase in success rate (Figs. 6A and 6B; 1 Hz AP firing), reflecting disinhibition of GABA release by blocking tonically active CB1 receptors (Neu et al., 2007). In NL3 KO synapses, strikingly, AM251 did not enhance IPSC amplitudes (Figs. 6A, S4A, and S4B) or success rates of synaptic transmission (Figs. 6B, S4A, and S4B). These findings suggest that IPSC amplitudes in the NL3 KO were larger because these synapses express higher release probabilities due to an apparent lack of tonic CB1 receptor activation.

To evaluate whether differences in the release probability alone, without other possible consequences of NL3 deletion, could explain the observed phenotype, we again used modeling and computer simulations. Fitting of the bin-averaged IPSC – successes data (Figs. 6C and S3A–S3C) resulted in similar Q and N estimates for the NL3 WT and KO data sets (mean and 95% confidence intervals; Q: 39 / 30.8–47.3 and 46.2 / 14.1–78.4 pA, and N: 5.6 / 4.1–7 and 4.4 / −2.9–11.8, for WT and NL3 KO, respectively). Using these parameter estimates in subsequent simulations (Figs. 6D and S3A–S3G), we found that the mean values of simulated IPSC – successes distributions were not significantly different from experimental values (inset in left panel) when P_R=0.12 (together with a σ_{PR}=0.19 and a

σ_Q=2; Q=39 pA and N=6 per model estimates) for NL3 WT, and when P_R=0.26 (together with a σ_{PR}=0.26 and a σ_Q=2.1; Q=46.2 pA and N=5 per model estimates) for NL3 KO. In addition, we quantified axonal bouton densities (Fig. 6E), which were not different between the two genotypes (WT: 0.18 ± 0.01 and NL3 KO: 0.18 ± 0.01, per μm, t-test, P=0.779). Together, these analyses suggest that the loss of tonic CB1 receptor activation, and the consequent ~2-fold increase in the probability of GABA release, is sufficient to account for the entire phenotype of the NL3 deletion at these synapses.

We next determined whether the loss of tonic CB1 receptor activation was affecting GABA release only from basket cell synapses, or whether all CB1-containing GABAergic synapses exhibit this phenotype. Thus, we repeated the CB1 receptor blocking experiments by monitoring IPSCs evoked by extracellular stimulation (which will cause GABA release from a broad set of presynaptic fibers that include CB1-receptor-containing axons). Application of AM251 again enhanced IPSCs in CA1 pyramidal cells, but consistently failed to do so in the NL3 KO (Fig. 6F). We also repeated these latter extracellular stimulation experiments with CP 945,598, a CB1 receptor antagonist that is structurally unrelated to AM251. Bath application of CP 945,598 (5 μM) replicated the findings with AM251 (Fig. 6G), independently confirming the absence of tonic EC signaling in NL3 KO mice.

Similar to the NL3 KO, paired recordings from slices prepared from the NL3 R451C KI mice revealed that the effect of AM251 on CCK basket cell IPSCs was greatly reduced (Figs. 6H and 6I). These data suggest that NL3 is essential for the tonic endocannabinoid signaling that inhibits GABA release from CCK basket cell synapses. Futhermore, we tested whether the NL3 KO may alter tonic CB1 receptor-mediated signaling at glutamatergic synapses. We stimulated Schaffer-collateral synapses and recorded from CA1 pyramidal cells (in the presence of 50 μM picrotoxin). However, bath application of AM251 (10 μM) failed to increase EPSC amplitudes in either WT slices or NL3 KO slices (Fig. 6J; see also Hoffmann et al., 2010). Together, these data suggest that NL3-related mutations may impair tonic endocannabinoid signaling at CB1 receptor-containing inhibitory, but not excitatory synapses.

NL3 is not required for phasic endocannabinoid signaling

A loss of tonic endocannabinoid signaling could be due to a specific ablation of tonic endocannabinoid secretion, or to a general block of all endocannabinoid secretion or endocannabinoid sensing, for example due to a removal of CB1 receptors. To differentiate between these possibilities, we examined phasic endocannabinoid signaling in NL3 KO mice. We first analyzed depolarization-induced suppression of inhibition (DSI). During DSI, depolarization of pyramidal neurons induces transient release of endocannabinoids, which retrogradely activate CB1 receptors, leading to powerful blockade of GABA release that can last for several seconds (Pitler and Alger, 1994; Wilson and Nicoll, 2001; Földy et al 2006). These experiments showed that the NL3 KO did not affect the magnitude or time course of DSI, documenting that CB1 receptors were properly localized and phasic endocannabinoid signaling was retained in NL3 KO mice (Fig. 7A). We also tested whether the NL3 KO alters the phasic endocannabinoid signaling that induces a long-term depression of inhibitory synapses (I-LTD; Chevaleyre and Castillo, 2003; reviewed in Castillo et al., 2011). High-frequency extracellular stimulation at the border of strata pyramidale and radiatum reliably induced I-LTD both in wild-type and in NL3 KO mice (Fig. 7B). Thus, the NL3 KO does not block two different forms of synaptic plasticity dependent on phasic endocannabinoid signaling.

DISCUSSION

In the present study, we systematically compared the synaptic effects of two different mutations in NL3 that are associated with autism, and examined in paired recordings inhibitory synapses that are formed by two classes of presynaptic basket cells onto the same class of postsynaptic pyramidal neurons in the hippocampus.

This study had two goals. The first goal was based on the lack of a common phenotype produced by the two NL3 mutations in mice, despite their shared association with autism in humans, prompting us to search for such a common phenotype. As a starting point in this search, we used the altered rate of spontaneous mini activity that we had previously identified in NL3 KO mice (Etherton et al., 2011a). We were led in this search by the notion that the lack of a similar phenotype in R451C-mutant synapses could have been due to confounding gain-of-function effects of the R451C substitution on other subsets of synapses on the same neuron, which may have occluded a common phenotype shared by the R451C KI and NL3 KO neurons. Thus, to search for common phenotypes, we used paired recordings which enabled us to separately monitor defined synapses originating from specific classes of inhibitory basket cells in the hippocampus.

The second goal of this study was stimulated by our earlier results demonstrating that the R451C substitution produced different synaptic phenotypes in distinct brain regions (Tabuchi et al., 2007; Etherton et al., 2011a). These results led us to test whether the NL3 KO and the R451C KI mutations might produce different phenotypes even in distinct synapses formed onto the same postsynaptic neuron. The differences in NL3 phenotypes in different brain regions supported the hypothesis that NL3 does not simply act in establishing synapses as such, but functions to specify synaptic properties depending on the presynaptic partner, a hypothesis that would predict that synapses formed by different presynaptic partners on the same postsynaptic neuron may also exhibit distinct changes in NL3 mutants.

Our study addresses both goals. The results suggest three major conclusions that have implications not only for autism pathophysiology, but also for synapse formation and synaptic endocannabinoid signaling.

First, we unexpectedly found that NL3 is essential for tonic but not phasic endocannabinoid signaling. The mechanisms of tonic endocannabinoid signaling are not well studied - in fact, its very existence as a specific process was unclear (Kim and Alger, 2010; Alger, 2012). Our finding that tonic endocannabinoid signaling is impaired in NL3 KO neurons (and R451C KI neurons) validates this form of endocannabinoid signaling as a specific regulatory process that is not an `accident' of endocannabinoid leakage or spillover, and identifies NL3 as the only protein known to be specifically required for tonic endocannabinoid secretion. The loss of tonic endocannabinoid signaling is the likely cause for the change in mini-frequency we previously observed in NL3 KO mice (Etherton et al., 2011a). The fact that this phenotype is caused by both the NL3 KO and R451C KI suggests that a loss of tonic endocannabinoid signaling may be a component of autism pathogenesis, and suggests new avenues for potential treatments (Cravatt and Lichtman, 2003; Piomelli, 2003; Katona and Freund, 2008). Although the mechanism by which NL3 acts in tonic endocannabinoid secretion is unknown, it seems likely that NL3 serves to localize the as yet unknown tonic secretory machinery to synapses via trans-synaptic interactions with neurexins. Alternatively, it is conceivable that the NL3 loss-of-function activates an enzyme that selectively degrades ligands of tonic but not the phasic endocannabinoid signal (Alger and Kim, 2011; Alger, 2012).

Second, the R451C mutation causes both gain- and loss-of-function effects (Fig. 8). We previously demonstrated that the R451C KI causes gain-of-function effects when we

compared the phenotype of the NL3 KO and R451C KI mutations in inhibitory synapses in the cortex and excitatory synapses in the hippocampus (Tabuchi et al., 2007; Etherton et al., 2011a). In these synapses, the NL3 KO elicited no major phenotype while the NL3 R451C KI produced specific increases in synaptic transmission. However, R451C loss-of-function effects were not detected in earlier studies, although they are consistent with the fact that the R451C mutation destabilizes NL3 and reduces its levels ~90% (De Jaco et al., 2010; Tabuchi et al., 2007). The present paper now shows that the R451C mutation does indeed also cause loss-of-function phenotypes, thereby reconciling the observation of both this mutation and a NL3 deletion in autism (Jamain et al., 2003; Sanders et al., 2011).

Third, the R451C mutation causes distinct effects on different types of synapses of the same postsynaptic neuron (Fig. 8). The differences between phenotypes induced by the R451C KI suggests that NL3 acts in a context-dependent manner not only in a regional sense (i.e., it has a different phenotype in cortical vs. hippocampal synapses), but also within a brain region. This observation argues against what might be called a `mechanical' view of synaptic cell adhesion whereby a molecule performs the same function in all contexts - instead, the observations on the R451C mutation reveal that NL3 can perform distinct functions, presumably depending on the ligands that are available in a given synapse, a result that is consistent with previous results obtained for neuroligin-2 (Gibson et al., 2009). Moreover, the inhibition of PV-containing synapses by the R451C substitution represents the first time the R451C mutation was found to decrease synaptic strength as in previous studies it always increased synaptic strength (Tabuchi et al., 2007; Etherton et al., 2011a). The powerful size of this effect is again consistent with a major regulatory function of neuroligins in synapses.

The multitude of the effects of the R451C mutation on neurotransmission (Fig. 8) is surprising and supports the notion that neuroligins participate in a balanced array of diverse functions, possibly via interactions with multiple ligands. Specifically, the R451C mutation may act by shifting the activity of NL3 in a fluid interaction network composed of multiple competing trans-synaptic ligands. Our previous studies suggested that at least neuroligin-1 functions as a trans-synaptic cell-adhesion molecule by binding both to neurexins and to as yet unidentified other ligands (Ko et al., 2009). It is possible that the R451C mutation blocks the binding of NL3 to one of the ligands, and/or activates the binding of another ligand, thereby shifting the interaction network.

Although we show here that NL3 is selectively essential for tonic endocannabinoid signaling, this result does not exclude the possibility that NL3 performs other functions. In fact, analogous to other genes such as RIMs (Kaeser et al., 2012), NL3 could perform major functions that are redundantly also performed by other neuroligins. The previous analysis of constitutive neuroligin triple KO mice strongly supports this notion by revealing functional redundancy among neuroligins (Varoqueaux et al., 2006), as does the observation of multiple strong phenotypes produced by the R451C and R704C KI mutations in NL3 (Tabuchi et al., 2007; Etherton et al., 2011a and 2011b). The requirement for NL3 in tonic endocannabinoid signaling affirms the notion that neuroligins specify synapse properties, as NL3 confers onto CCK-containing synapses tonic endocannabinoid signaling without influencing phasic signaling or other synaptic parameters. Tonic endocannabinoid signaling was not previously associated with a specific regulatory mechanism but the link to NL3 revealed here validates the importance of this signaling pathway and suggests a possible endocannabinoid involvement in autism.

EXPERIMENTAL PROCEDURES

Mouse breeding and genotyping

Mice were genotyped as described previously (Tabuchi et al., 2007, Etherton et al., 2011a). All animal protocols and husbandry practices were approved by the Institutional Animal Care and Use Committee at Stanford University.

Electrophysiology

Hippocampal slices (300 μm) were prepared from 3–4 weeks old NL3 R451C KI and NL3 KO mice. Slices were incubated at 33 °C in sucrose-containing artificial cerebrospinal fluid (ACSF; 85 mM NaCl, 75 mM sucrose, 2.5 mM KCl, 25 mM glucose, 1.25 mM NaH_2PO_4, 4 mM $MgCl_2$, 0.5 mM $CaCl_2$ and 24 mM $NaHCO_3$) for an hour and than incubated in the same solution at room temperature until recording. Electrophysiological recordings were made in ACSF containing 126 mM NaCl, 2.5 mM KCl, 10 mM glucose, 1.25 mM NaH_2PO_4, 2 mM $MgCl_2$, 2 mM $CaCl_2$ and 26 mM $NaHCO_3$. Slices were visualized in an upright microscope (Olympus, BX-61WI) with infrared differential interference contrast optics. Whole cell recordings were obtained from the interneurons with patch pipettes (King Precision Glass, Inc., 3–5 MΩ) filled with internal solution containing 126 mM K-gluconate, 4 mM KCl, 10 mM HEPES, 4 mM Mg-ATP, 0.3 Na-GTP, 10 mM phosphocreatine and 0.2% biocytin (pH 7.2, 270–290 mOsm), and from postsynaptic pyramidal cells containing 40 mM CsCl, 90 mM K-gluconate, 1.8 mM NaCl, 1.7 mM $MgCl_2$, 3.5 mM KCl, 0.05 mM EGTA, 10 mM HEPES, 2 mM Mg-ATP, 0.4 mM Na-GTP, 10 mM phosphocreatine (pH 7.2, 270–290 mOsm; in some of the recordings 0.2% biocytin was also added to this solution). All electrophysiological recordings were made at 33 °C, using MultiClamp700B amplifiers (Molecular Devices, Sunnyvale, CA). Signals were filtered at 4 kHz using Bessel filter and digitized at 10 kHz with a Digidata 1440A analog-digital interface (Molecular Devices, Sunnyvale, CA). Series resistance was monitored, and recordings were discarded if the series resistance changed significantly or reached 25 MΩ. The recorded traces were analyzed using Clampfit software (Molecular Devices, Sunnyvale, CA). PV and CCK interneurons were distinguished based on their distinct electrophysiological spiking properties (Földy et al., 2010), and by the presence of DSI in CCK basket cell synapses (see Fig. 7A). IPSCs were individually inspected and included in the analysis based on their onset latency following the presynaptic action potential. For statistical analysis Student's t-test, paired t-test or Mann-Whitney Rank Sum Test (RST) was used, and data are presented as mean ± s.e.m., unless noted otherwise; significance was $P < 0.05$.

Quantal model

Individual basket cells innervate postsynaptic pyramidal cells via multiple release sites (N; Biró et al., 2006; Földy et al., 2010), in which intrinsically variable synaptic parameters (such as quantal size and release probability; Q and P_R respectively) produce a trial-to-trial fluctuation in the IPSC amplitudes. The distribution of these fluctuations can be described by models that are based on binomial statistics and allow estimates of Q and N (Silver, 2003, Biró et al., 2006). In this study, we ought to extend quantal modeling to analyze pooled data from multiple paired-recording experiments of defined synapse populations, and extract mean quantal information that is characteristic to each population. For modeling, we analyzed synapses by quantifying IPSC amplitudes and success rates. Assuming that each synapse population can be described by characteristic mean N and Q values, it is reasonable to assume that the pair-to-pair variability in IPSC amplitudes and success rates is dominated by variability in P_R. In this case, the distribution of IPSC amplitudes and success rates should follow the $\left[\mathrm{PSC}=Q\cdot N\cdot\left[1-\sqrt[N]{1-\mathrm{Successes}}\right]\right.$ model (Eq. 1; see Fig. S2 for more information). For fitting the IPSC model on experimental data, to estimate quantal

parameters, we employed the built-in, unconstrained *NonlinearModelFit* algorithm in Mathematica 8 (Wolfram Research, Inc., Champaign, IL). Note that the basic assumptions of this approach (i.e. the existence of characteristic Q and N values in each synapse population) were supported by the similarity between the observed and predicted IPSC distributions (Eq.1; see Figs. 5A and 6C).

Computational model

In order to gain further qualitative insight into how pre- and postsynaptic changes may contribute to the synaptic phenotypes produced by NL3 mutations, we devised a simple computational model that incorporated five modifiable synaptic parameters: the number of release sites (N) and the mean and variance of the release probability (P_R and σ_{PR}, respectively) and of quantal IPSCs (Q and σ_Q, respectively). Note that non-zero variances were necessary to simulate variability both in the number of successful transmissions (by σ_{PR}) and IPSC amplitudes (by σ_Q). To initialize the simulations, p_i values (that is the release probability of the *i*-th release site) were assigned randomly from a normal probability distribution function with P_R mean and σ_{PR} variance for each release site. In addition, for each release site, q_i values (that is the quantal size in the *i*-th release site) were randomly assigned from a log-normal probability distribution function of mean Q and σ_Q variance parameters (see Supplementary Fig. S3 for more information). Computational IPSCs (cIPSCs) and successes (cSuccesses) were derived as described in the text. For each condition, estimates of Q and N were adopted from the quantal model (Fig. 5A and 6C). Each simulation had the same sample size as the original data, and each simulation was repeated 50 times with random assignments of new p_i and q_i values. For statistical comparisons, we tested the null-hypothesis that the difference between the mean computed and experimental successes and IPSCs were zero; simulation parameters were accepted when $P>0.05$ using Student's t-test. To estimate the robustness of the resulting simulation parameters, we quantified an average range for each parameter which still justifies the null-hypothesis: $\Delta P_R=\pm 0.006$, $\Delta\sigma_{PR}=\pm 0.09$, $\Delta Q=\pm 0.7$ pA and $\Delta\sigma_Q=\pm 0.06$ pA (relative to values presented in the main text). Parameter deviations beyond these ranges independently resulted in statistically significant differences ($P<<0.05$) between the simulated and experimental distributions. Simulations were implemented and run using Mathematica 8 (Wolfram Research, Inc.).

Neuroanatomy

After recordings, all slices were transferred into a fixative solution containing 4% paraformaldehyde and 0.2% picric acid in 0.1 M phosphate buffer. In order to examine the axonal and dendritic arbor of presynaptic basket cell, biocytin-filled cells were visualized after recordings with 3,3-diaminobenzidinetetrahydrochloride (0.015%) using PK-6100 DAB and Vectastain SK-4100 ABC kit (Vector Laboratories, Burlingame, CA). Example basket cells in Figures 1 and 2 were reconstructed using Neurolucida 10 (MBF Bioscience, Williston, VT). For axonal bouton density quantification, axonal segments with corresponding boutons were reconstructed using Neurolicida 10. The length of the axons (which averaged 1180.4±128.4 μm, mean length ± s.e.m., in the reconstructed cells) and bouton numbers were determined using NeuroExplorer (MBF Bioscience, Williston, VT).

Supplementary Material

Refer to Web version on PubMed Central for supplementary material.

Acknowledgments

We would like to thank Nathan Huang, Scarlett Fang, Ayeh Darvishzadeh and Shaon Ghosh for technical assistance, and Dr. Jason Aoto for advice. This study was supported by grants from the Simons Foundation (177850 to TCS), the NIMH (P50 MH086403 to RCM and TCS), the NIDA (K99DA034029 to CF), and the NINDS (NS069375 to the Stanford Neuroscience Microscopy Service).

REFERENCES

Ali AB, Todorova M. Asynchronous release of GABA via tonic cannabinoid receptor activation at identified interneuron synapses in rat CA1. Eur. J. Neurosci. 2010; 31:1196–1207. [PubMed: 20345910]

Alger BE. Retrograde signaling in the regulation of synaptic transmission: focus on endocannabinoids. Prog. Neurobiol. 2002; 68:247–286. [PubMed: 12498988]

Alger BE, Kim J. Supply and demand for endocannabinoids. Trends Neurosci. 2011; 34:304–315. [PubMed: 21507493]

Alger BE. Endocannabinoids at the synapse a decade after the dies mirabilis (29 March 2001): what we still do not know. J. Physiol. 2012; 590:2203–2212. [PubMed: 22289914]

Bartos M, Vida I, Jonas P. Synaptic mechanisms of synchronized gamma oscillations in inhibitory interneuron networks. Nat. Rev. Neurosci. 2007; 8:45–56. [PubMed: 17180162]

Biró AÁ, Holderith NB, Nusser Z. Release probability-dependent scaling of the postsynaptic responses at single hippocampal GABAergic synapses. J. Neurosci. 2006; 26:12487–12496. [PubMed: 17135411]

Baudouin SJ, Gaudias J, Gerharz S, Hatstatt L, Zhou K, Punnakkal P, Tanaka KF, Spooren W, Hen R, De Zeeuw CI, Vogt K, Scheiffele P. Shared synaptic pathophysiology in syndromic and nonsyndromic rodent models of autism. Science. 2012; 338:128–132. [PubMed: 22983708]

Budreck EC, Scheiffele P. Neuroligin-3 is a neuronal adhesion protein at GABAergic and glutamatergic synapses. Eur. J. Neurosci. 2007; 26:1738–1748. [PubMed: 17897391]

Castillo PE, Chiu CQ, Carroll RC. Long-term plasticity at inhibitory synapses. Curr. Opin. Neurobiol. 2011; 21:328–338. [PubMed: 21334194]

Chadman KK, Gong S, Scattoni ML, Boltuck SE, Gandhy SU, Heintz N, Crawley JN. Minimal aberrant behavioral phenotypes of NL3 R451C knockin mice. Autism Res. 2008; 1:147–158. [PubMed: 19360662]

Chevaleyre V, Castillo PE. Heterosynaptic LTD of hippocampal GABAergic synapses: a novel role of endocannabinoids in regulating excitability. Neuron. 2003; 38:461–472. [PubMed: 12741992]

Chubykin AA, Atasoy D, Etherton MR, Brose N, Kavalali ET, Gibson JR, Südhof TC. Activity-dependent validation of excitatory versus inhibitory synapses by neuroligin-1 versus neuroligin-2. Neuron. 2007; 54:919–931. [PubMed: 17582332]

Cravatt BF, Lichtman AH. Fatty acid amide hydrolase: an emerging therapeutic target in the endocannabinoid system. Curr. Opin. Chem. Biol. 2003; 7:469–475. [PubMed: 12941421]

De Jaco A, Dubi N, Comoletti D, Taylor P. Folding anomalies of NL3 caused by a mutation in the alpha/beta-hydrolase fold domain. Chem. Biol. Interact. 2010; 187:56–58. [PubMed: 20227402]

Etherton MR, Blaiss CA, Powell CM, Südhof TC. Mouse neurexin-1alpha deletion causes correlated electrophysiological and behavioral changes consistent with cognitive impairments. Proc. Natl. Acad. Sci. USA. 2011a; 106:17998–18003. [PubMed: 19822762]

Etherton MR, Tabuchi K, Sharma M, Ko J, Südhof TC. An autism-associated point mutation in the neuroligin cytoplasmic tail selectively impairs AMPA receptor-mediated synaptic transmission in hippocampus. EMBO J. 2011b; 30:2908–2919. [PubMed: 21642956]

Földy C, Neu A, Jones MV, Soltesz I. Presynaptic, activity-dependent modulation of cannabinoid type 1 receptor-mediated inhibition of GABA release. J. Neurosci. 2006; 26:1465–1469. [PubMed: 16452670]

Földy C, Lee SH, Morgan RJ, Soltesz I. Regulation of fast-spiking basket cell synapses by the chloride channel ClC-2. Nat. Neurosci. 2010; 13:1047–1049. [PubMed: 20676104]

Freund TF. Interneuron Diversity series: Rhythm and mood in perisomatic inhibition. Trends Neurosci. 2003; 26:489–495. [PubMed: 12948660]

Freund TF, Katona I, Piomelli D. Role of endogenous cannabinoids in synaptic signaling. Physiol. Rev. 2003; 83:1017–1066. [PubMed: 12843414]

Freund TF, Katona I. Perisomatic inhibition. Neuron. 2007; 56:33–42. [PubMed: 17920013]

Gibson JR, Huber KM, Südhof TC. Neuroligin-2 deletion selectively decreases inhibitory synaptic transmission originating from fast-spiking but not from somatostatin-positive interneurons. J. Neurosci. 2009; 29:13883–13897. [PubMed: 19889999]

Glickfeld LL, Atallah BV, Scanziani M. Complementary modulation of somatic inhibition by opioids and cannabinoids. J. Neurosci. 2008; 28:1824–1832. [PubMed: 18287499]

Graf ER, Zhang X, Jin SX, Linhoff MW, Craig AM. Neurexins induce differentiation of GABA and glutamate postsynaptic specializations via neuroligins. Cell. 2004; 119:1013–1026. [PubMed: 15620359]

Hentges ST, Low MJ, Williams JT. Differential regulation of synaptic inputs by constitutively released endocannabinoids and exogenous cannabinoids. J. Neurosci. 2005; 25:9746–9751. [PubMed: 16237178]

Hoffman AF, Laaris N, Kawamura M, Masino SA, Lupica CR. Control of cannabinoid CB1 receptor function on glutamate axon terminals by endogenous adenosine acting at A1 receptors. J. Neurosci. 2010; 30:545–555. [PubMed: 20071517]

Hoon M, Soykan T, Falkenburger B, Hammer M, Patrizi A, Schmidt KF, Sassoè-Pognetto M, Löwel S, Moser T, Taschenberger H, et al. Neuroligin-4 is localized to glycinergicpostsynapses and regulates inhibition in the retina. Proc. Natl. Acad. Sci. USA. 2011; 108:3053–3058. [PubMed: 21282647]

Ichtchenko K, Hata Y, Nguyen T, Ullrich B, Missler M, Moomaw C, Südhof TC. Neuroligin 1: a splice site-specific ligand for beta-neurexins. Cell. 1995; 81:435–443. [PubMed: 7736595]

Ichtchenko K, Nguyen T, Südhof TC. Structures, alternative splicing, and neurexin binding of multiple neuroligins. J. Biol. Chem. 1996; 271:2676–2682. [PubMed: 8576240]

Jamain S, Quach H, Betancur C, Råstam M, Colineaux C, Gillberg IC, Soderstrom H, Giros B, Leboyer M, Gillberg C, Bourgeron T, Paris Autism Research International Sibpair Study. Mutations of the X-linked genes encoding neuroligins NLGN3 and NLGN4 are associated with autism. Nat. Genet. 2003; 34:27–29. [PubMed: 12669065]

Kaeser PS, Deng L, Fan M, Südhof TC. RIM Genes differentially contribute to organizing presynaptic release sites. Proc. Natl. Acad. Sci. USA. 2012; 109:11830–11835. [PubMed: 22753485]

Katona I, Freund TF. Endocannabinoid signaling as a synaptic circuit breaker in neurological disease. Nat. Med. 2008; 14:923–930. [PubMed: 18776886]

Katona I, Freund TF. Multiple functions of endocannabinoid signaling in the brain. Annu. Rev. Neurosci. 2012; 35:529–558. [PubMed: 22524785]

Kim J, Alger BE. Reduction in endocannabinoid tone is a homeostatic mechanism for specific inhibitory synapses. Nat. Neurosci. 2010; 13:592–600. [PubMed: 20348918]

Klausberger T, Marton LF, O'Neill J, Huck JH, Dalezios Y, Fuentealba P, Suen WY, Papp E, Kaneko T, Watanabe M, et al. Complementary roles of cholecystokinin- and parvalbumin-expressing GABAergic neurons in hippocampal network oscillations. J. Neurosci. 2005; 25:9782–9793. [PubMed: 16237182]

Klausberger T, Somogyi P. Neuronal diversity and temporal dynamics: the unity of hippocampal circuit operations. Science. 2008; 321:53–57. [PubMed: 18599766]

Ko J, Fuccillo MV, Malenka RC, Südhof TC. LRRTM2 functions as a neurexin ligand in promoting excitatory synapse formation. Neuron. 2009; 64:791–798. [PubMed: 20064387]

Lisman JE, Coyle JT, Green RW, Javitt DC, Benes FM, Heckers S, Grace AA. Circuit-based framework for understanding neurotransmitter and risk gene interactions in schizophrenia. Trends Neurosci. 2008; 31:234–242. [PubMed: 18395805]

Losonczy A, Biró AA, Nusser Z. Persistently active cannabinoid receptors mute a subpopulation of hippocampal interneurons. Proc. Natl. Acad. Sci. USA. 2004; 101:1362–1367. [PubMed: 14734812]

Neu A, Földy C, Soltesz I. Postsynaptic origin of CB1-dependent tonic inhibition of GABA release at cholecystokinin-positive basket cell to pyramidal cell synapses in the CA1 region of the rat hippocampus. J. Physiol. 2007; 578:233–47. [PubMed: 17053036]

Piomelli D. The molecular logic of endocannabinoid signalling. Nat. Rev. Neurosci. 2003; 4:873–884. [PubMed: 14595399]

Pitler TA, Alger BE. Depolarization-induced suppression of GABAergic inhibition in rat hippocampal pyramidal cells: G protein involvement in a presynaptic mechanism. Neuron. 1994; 13:1447–1455. [PubMed: 7993636]

Poulopoulos A, Aramuni G, Meyer G, Soykan T, Hoon M, Papadopoulos T, Zhang M, Paarmann I, Fuchs C, Harvey K, et al. Neuroligin 2 drives postsynaptic assembly at perisomatic inhibitory synapses through gephyrin and collybistin. Neuron. 2009; 63:628–642. [PubMed: 19755106]

Sanders SJ, Ercan-Sencicek AG, Hus V, Luo R, Murtha MT, Moreno-De-Luca D, Chu SH, Moreau MP, Gupta AR, Thomson SA, et al. Multiple recurrent de novo CNVs, including duplications of the 7q11.23 Williams syndrome region, are strongly associated with autism. Neuron. 2011; 70:863–885. [PubMed: 21658581]

Silver RA. Estimation of nonuniform quantal parameters with multiple-probability fluctuation analysis: theory, application and limitations. J. Neurosci. Methods. 2003; 130:127–41. [PubMed: 14667542]

Song JY, Ichtchenko K, Südhof TC, Brose N. Neuroligin 1 is a postsynaptic cell-adhesion molecule of excitatory synapses. Proc. Natl. Acad. Sci. USA. 1999; 96:1100–1105. [PubMed: 9927700]

Südhof TC. Neuroligins and neurexins link synaptic function to cognitive disease. Nature. 2008; 455:903–911. [PubMed: 18923512]

Szabó GG, Holderith N, Gulyás AI, Freund TF, Hájos N. Distinct synaptic properties of perisomatic inhibitory cell types and their different modulation by cholinergic receptor activation in the CA3 region of the mouse hippocampus. Eur. J. Neurosci. 2010; 31:2234–2246. [PubMed: 20529124]

Tabuchi K, Blundell J, Etherton MR, Hammer RE, Liu X, Powell CM, Südhof TC. A NL3 mutation implicated in autism increases inhibitory synaptic transmission in mice. Science. 2007; 318:71–76. [PubMed: 17823315]

Varoqueaux F, Aramuni G, Rawson RL, Mohrmann R, Missler M, Gottmann K, Zhang W, Südhof TC, Brose N. Neuroligins determine synapse maturation and function. Neuron. 2006; 51:741–754. [PubMed: 16982420]

Wilson RI, Nicoll RA. Endogenous cannabinoids mediate retrograde signalling at hippocampal synapses. Nature. 2001; 410:588–592. [PubMed: 11279497]

Zhang C, Milunsky JM, Newton S, Ko J, Zhao G, Maher TA, Tager-Flusberg H, Bolliger MF, Carter AS, et al. A neuroligin-4 missense mutation associated with autism impairs neuroligin-4 folding and endoplasmic reticulum export. J. Neurosci. 2009; 29:10843–10854. [PubMed: 19726642]

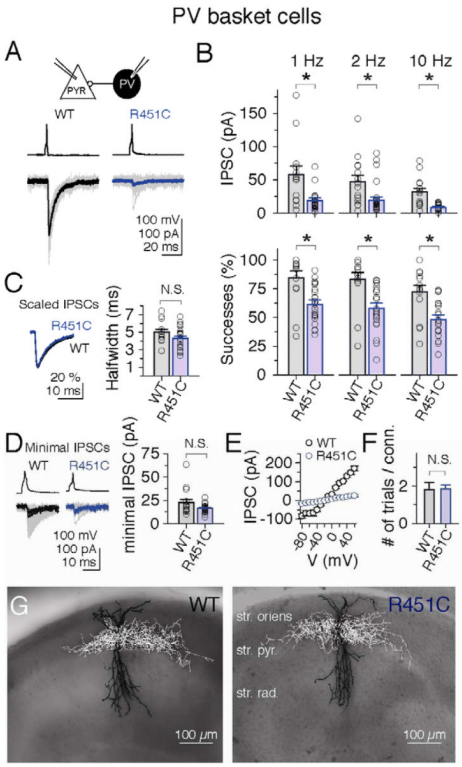

Figure 1. Neuroligin-3 R451C substitution impairs GABAergic synaptic transmission in PV basket cell synapses

(A) Paired recordings of presynaptic APs in PV basket cells (upper traces) that produce unitary IPSCs in CA1 pyramidal cells (lower traces, $V_{holding}$ = −70 mV). **(B)** Comparison of IPSC amplitudes (including failures) and of the percentages of successful transmissions induced by presynaptic APs applied at 1, 5, and 10 Hz in wild-type and R451C-mutant synapses. Open circles represent individual pairs (n_{WT}=14, n_{R451C}=27, Mann-Whitney RST, P<0.02 for all data sets). **(C)** The R451C KI mutation did not alter the half width of IPSCs (n_{WT}=14, n_{R451C}=23, Mann-Whitney RST, P=0.092). **(D)** Quantification of minimal IPSCs (amplitude of reliably occurring smallest IPSCs in each pair) suggest no change in quantal response in the R451C KI (n_{WT}=15, n_{R451C}=25, Mann-Whitney RST, P=0.235). **(E)** Additional paired-recordings show that IPSCs was independent of post-synaptic membrane voltage in R451C KI mice (n_{WT}=3, n_{R451C}=4). **(F)** The frequency of finding synaptically coupled pairs was not altered in R451C mice. **(G)** Neurolucida reconstructions of biocytin-filled basket cells show major reorganization in axonal and dendritic arbor of PV basket cells (str. = stratum, pyr. = pyramidale, rad. = radiatum). See also Figure S1.

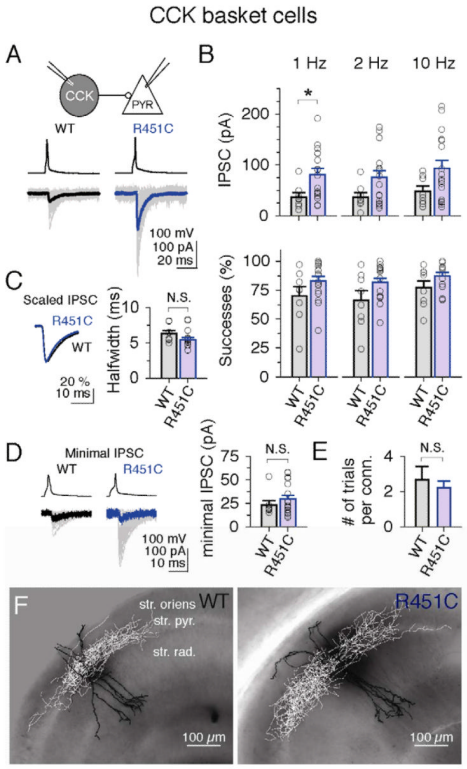

Figure 2. Neuroligin-3 R451C substitution enhances GABAergic synaptic transmission in CCK basket cell synapses

(A) Paired recordings of presynaptic APs in CCK basket cells (upper traces) that produce unitary IPSCs in CA1 pyramidal cells (lower traces, $V_{holding}$ = −70 mV). **(B)** Comparison of IPSC amplitudes (including failures) and of the percentages of successful transmissions induced by presynaptic APs applied at 1, 5, and 10 Hz in wild-type and R451C-mutant synapses. Open circles represent individual pairs (n_{WT}=8, n_{R451C}=17, Mann-Whitney RST, P=0.013 at 1 Hz IPSCs and P>0.08 in all other data sets). **(C** & **D)** No change in IPSC halfwidth (n_{WT}=8, n_{R451C}=15, Mann-Whitney RST, P=0.098) and no increase in the minimal IPSC amplitudes in R451C KI (n_{WT}=8, n_{R451C}=15, Mann-Whitney RST, P=0.5) suggest that the enhanced IPSC amplitudes in R451C KIs is not due to changes in quantal GABA receptor responses. **(E)** The frequency of finding synaptically coupled pairs was not altered in R451C mice. **(F)** Neurolucida reconstructions of biocytin-filled basket cells show no major reorganization in axonal and dendritic arbor of CCK basket cells.

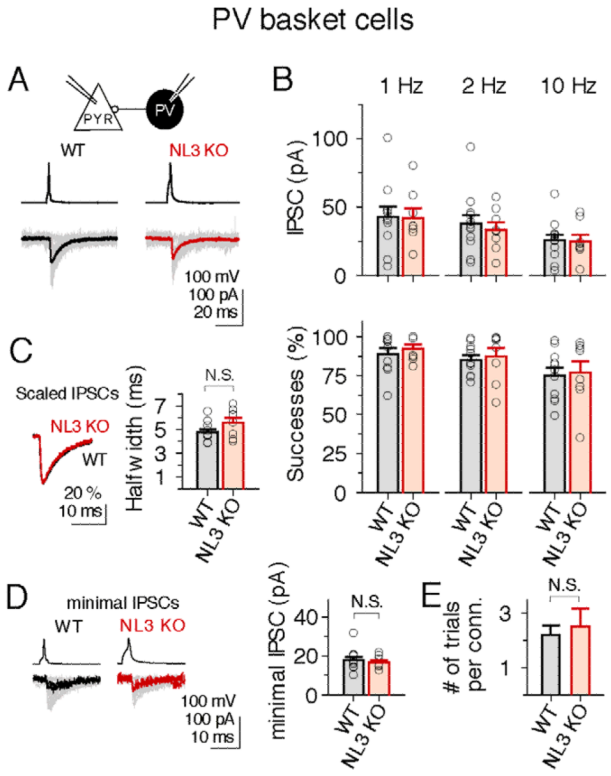

Figure 3. Neuroligin-3 KO does not alter GABAergic transmission in PV basket cell synapses

(A & **B)** Paired-recording data show that IPSC amplitudes and transmission rates were unaltered in NL3 KO mice compared to WT littermates (n_{WT}=12, n_{KO}=8, Mann-Whitney RST, P>0.32 in all data set). **(C** & **D)** Quantification of IPSC halfwidth and minimal IPSC amplitudes suggest no changes in postsynaptic GABA receptor subunit composition. **(E)** The frequency of finding connected pairs was similar in NL3 WT and KO mice.

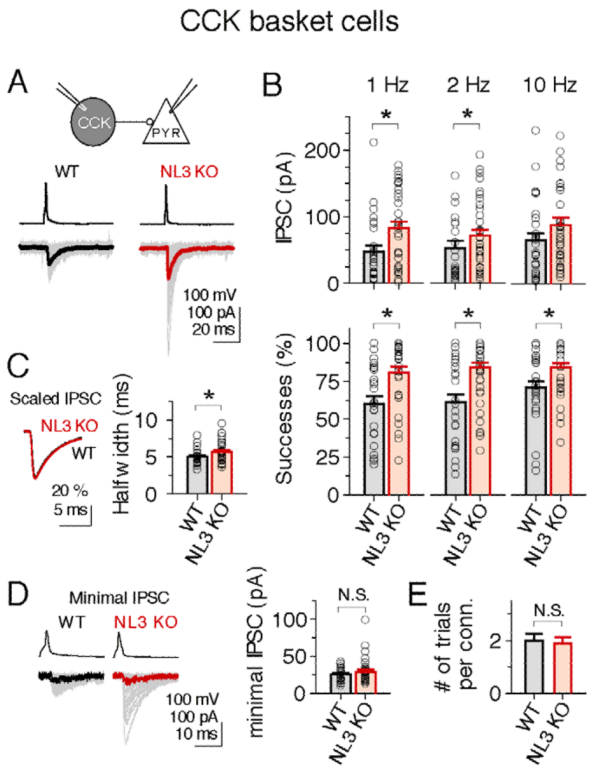

Figure 4. Neuroligin-3 KO enhances GABAergic synaptic transmission in CCK basket cell synapses similar to the R451C KI

(A & **B)** Paired recording data show that IPSC amplitudes and transmission rates were enhanced in CCK basket cell to CA1 pyramidal neuron synapses at multiple AP firing frequencies (n_{WT}=28, n_{KO}=36, Mann-Whitney RST, P=0.12 at 10 Hz IPSCs, and P<0.03 for all other data set). **(C)** Increase in IPSC halfwidth in KO suggest possible subunit reorganization of GABA receptor subunits in NL3 KO (n_{WT}=28, n_{KO}=35, Mann-Whitney RST, P=0.021). **(D** & **E)** No change in minimal IPSC amplitudes (n_{WT}=28, n_{KO}=35, Mann-Whitney RST, P=0.885), and in the frequency of finding connected pairs between CCK basket cells and pyramidal cells.

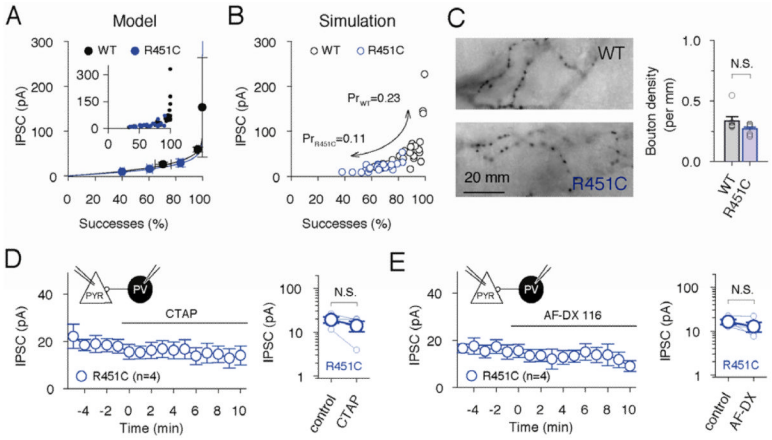

Figure 5. The NL3 R451C KI mutation lowers the probability of GABA release from PV basket cell synapses

(A) Averaged PV basket cell IPSCs (same data as in Fig. 1) are plotted against their corresponding averaged success rates (WT data were pooled from wild-type littermates of R451C KI and NL3 KO mice). Data were fitted to the equation $\left[\mathrm{PSC}=Q\cdot N\cdot\left[1-\sqrt[N]{1-\mathrm{Successes}}\right]\right.$ to estimate the mean quantal size (Q) and number of release sites (N) for each synapse population. Solid lines indicate best fit (black: WT, blue: R451C KI). Inset shows the distribution of individual data points. **(B)** Computer simulations of PV basket cell IPSCs. Simulation results for WT (open black circles) and R451C KI (open blue circles) were not significantly different (in mean IPSCs and successes) from their corresponding experimental IPSCs datasets when P_R was set to 0.23 and 0.11, respectively, in the model (see main text for further parameters). **(C)** Light microscopy analysis of the bouton density of PV basket cell axons. Left: example of axonal segments for axons in WT and R451C KI mice. Right: summary data from WT (n=7) and R451C KI (n=8) mice. P=0.152, Mann-Whitney RST. **(D)** Bath application of μ-opioid receptor antagonist CTAP (500 nM) in paired recording experiments between PV basket and pyramidal cells in R451C KI mice (n=4 pairs). Averaged time course (left) and time averaged means (right) of the 4 recordings did not show statistically significant effect of μ-opioid receptor antagonist on IPSCs. **(E)** Bath application of M2 muscarinic-receptor antagonist AF-DX 116 (10 μM) in paired recording experiments between PV basket and pyramidal cells in R451C KI mice (n=4 pairs). Averaged time course (left) and time averaged means (right) of the 4 recordings did not show statistically significant effect of μ-opioid receptor antagonist on IPSCs. Averaged data presented as mean ± s.e.m. See also Figure S2 and S3.

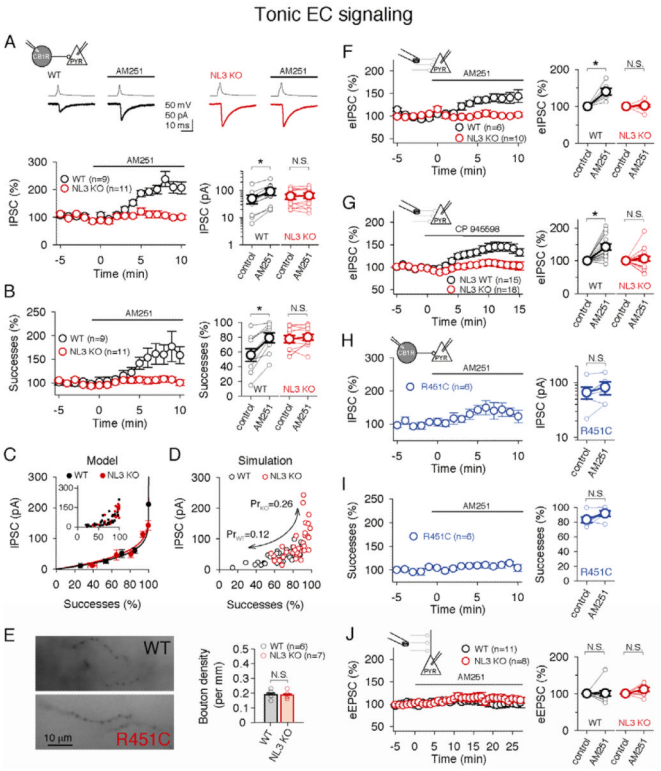

Figure 6. Neuroligin-3 KO and R451C KI mutations impair tonic endocannabinoid signaling

(A) Representative paired recordings (upper traces) and normalized time-courses (lower left panel) demonstrate that bath application of 10 μM AM251 enhances IPSCs in WT, but not in NL3 KO mice. Lower right panel: IPSC changes (failures included) in each paired-recording experiment (`control': average data for minutes 1–5, `AM251': for minutes 6–10; n_{WT}=9, P=0.004; n_{NL3KO}=11, P=0.268, paired T-test). **(B)** Left panel: time-courses of AM251 wash-in suggest that the lack of effect of AM251 on IPSCs was due to the failure of AM251 in increasing the number of successful transmissions. Right panel: AM251 reliably increased the number of successes in WT, but not in NL3 KO mice (n_{WT}=9, P<0.001; n_{NL3KO}=11, P=0.79, paired T-test). **(C)** Averaged CCK basket cell IPSCs (same data as in Fig. 4) are plotted against their corresponding averaged success rates (WT data were pooled from wild-type littermates of R451C KI and NL3 KO mice). Data were fitted to the equation $\left[\mathrm{PSC}=Q\cdot N\cdot\left[1-\sqrt[N]{1-\mathrm{Successes}}\right]\right.$ to estimate the mean quantal size (Q) and number of release sites (N) for each synapse population. Solid lines indicate best fit (black: WT, red: NL3 KO). Inset shows the distribution of individual data points. **(D)** Computer simulations of CCK basket cell IPSCs. Simulation results for WT (open black circles) and NL3 KO (open red circles) were not significantly different (in mean IPSCs and successes) from their corresponding experimental IPSCs datasets when P_R was set to 0.26 and 0.12, respectively, in the model (see main text for further parameters). **(E)** Light microscopy analysis of the bouton density of CCK basket cell axons. Left: example of axonal segments for axons in WT and NL3 KO mice. Right: summary data from WT (n=6) and NL3 KO (n=7) mice. P=0.779, t-test. **(F)** Time-course of the effect of the AM251 wash-in on extracellulary evoked IPSCs (eIPSC; left panel), and averaged data in each experiment (right panel) show increase in eIPSC amplitude in WT, but not in NL3 KO mice ($V_{pyramidal}$= −70 mV, 1 Hz stimulation, in the presence of 5 μM NBQX and 10 μM D-AP5; n_{WT}=6, P=0.008; n_{NL3KO}=10, P=0.63, paired t-test). **(G)** Time-course of the effect of the CP945598 wash-in on extracellulary evoked IPSCs (eIPSC; left panel), and averaged data in each experiment

(right panel) show increase in eIPSC amplitude in WT, but not in NL3 KO mice ($V_{pyramidal}$= −70 mV, 1 Hz stimulation, in the presence of 5 μM NBQX and 10 μM D-AP5; n_{WT}=15, P=0.0005; n_{NL3KO}=18, P=0.41, paired t-test). **(H** & **I)** Paired recordings of IPSC amplitudes and success rates in response to 10 μM AM251 in R451C KI mice. Left panels: time-course of the experiments. Right panels: absolute changes in each pair (n_{WT}=6, P=0.07; n_{R451C}=10, P=0.072, paired T-test). **(J)** Time-course of the effect of 10 μM AM251 wash-in on extracellularly evoked EPSCs (eEPSC; left panel), and averaged data in each experiment (right panel) in WT and NL3 KO mice ($V_{pyramidal}$= −70 mV, 1 Hz stimulation, in the presence of 50 μM picrotoxin; n_{WT}=11, P>0.05; n_{NL3KO}=8, P>0.05, paired t-test). See also Figure S2, S3 and S4.

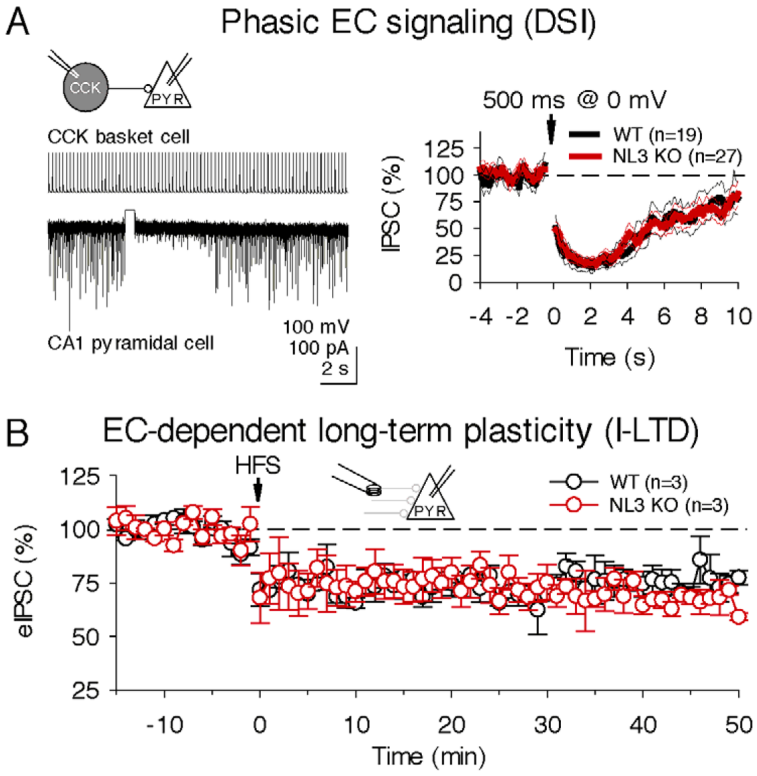

Figure 7. Neuroligin-3 is not required for phasic short-term endocannabinoid signaling (DSI) or long-term endocannabinoid-dependent synaptic plasticity (i-LTD)

(A) Paired recordings show that DSI induced by phasic endocannabinoid signaling was unaffected in NL3 KO (left panel: example of DSI, note the transient suppression of IPSCs after brief depolarization in the pyramidal cell; right panel: averaged time-course of DSI in WT and NL3 KO). **(B)** Deletion of NL3 does not affect the magnitude or time-course of the endocannabinoid-dependent I-LTD ($V_{pyramidal}$ = +10 mV, inter-stimulus interval 20 s, $[Cl_{pipette}]$ = 4 mM, in presence of 5 μM NBQX and 10 μM D-AP5).

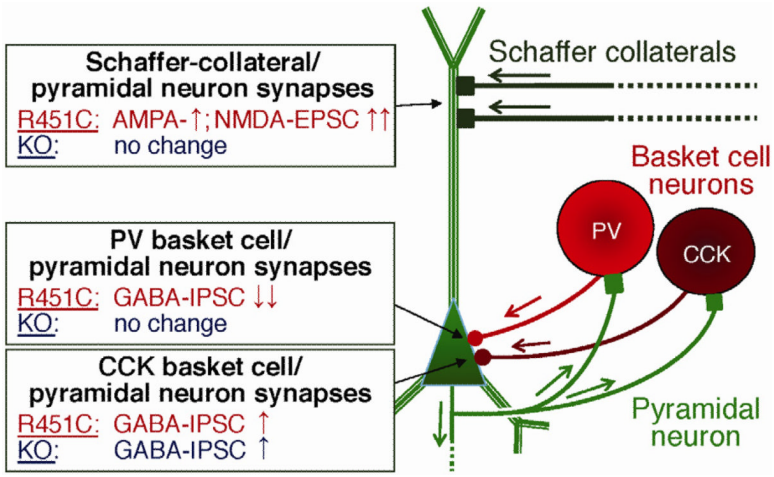

Figure 8. Schematic summary diagram of the effects of the NL3 KO and R451C substitution on three different synapses on pyramidal neurons in the CA1 region of the hippocampus

The diagram depicts a pyramidal neuron (green) receiving inputs from Schaffer collateral fibers and two different types of basket cell neurons (PV, parvalbumin; CCK, cholecystokinin). The changes observed in NL3 R451C knockin and KO mice are described on the left.